Crystal Structures and Magnetic Properties of $CuX_2(pdmp)_2$ Complexes (X = Br, Cl)

Antonio J. Costa-Filho,[†] Claudia E. Munte,[†] Claudio Barberato,[†] Eduardo E. Castellano,[†] M. P. D. Mattioli,[‡] Rafael Calvo,[§] and Otaciro R. Nascimento*,[†]

Instituto de Física de São Carlos, Universidade de São Paulo, CP 369, 13560-970 São Carlos, SP, Brazil, Instituto de Química de Araraquara, UNESP, CP 174, 14800 Araraquara, SP, Brazil, and Facultad de Bioquímica y Ciencias Biológicas, Universidad Nacional del Litoral and INTEC (CONICET-UNL), Güemes 3450, 3000 Santa Fe, Argentina

Received February 26, 1999

We report the synthesis and the structural and magnetic characterization of two new compounds: dibromobis(pdmp)copper(II), $CuBr_2C_{22}H_{24}N_4$ (**1**), and dichlorobis(pdmp)copper(II), $CuCl_2C_{22}H_{24}N_4$ (**2**), where pdmp = 1-phenyl-3,5-dimethylpyrazole. The structures were refined by full-matrix least-squares techniques to R1 = 0.0620 and 0.0777, respectively. Compound **1** belongs to the space group $P2_1/n$ with $a = 8.165(5)$ Å, $b = 10.432(3)$ Å, $c = 13.385(4)$ Å, $\beta = 100.12(4)°$, and $Z = 2$. Compound **2** belongs to the space group $P2_1/c$ with $a = 8.379(2)$ Å, $b = 22.630(2)$ Å, $c = 12.256(2)$ Å, $\beta = 98.43(3)°$, and $Z = 4$. It has the same molecular formula as a compound reported previously but a different crystal structure. Detailed single-crystal EPR measurements were performed for single-crystal samples of **1** and **2** at 9 and 35 GHz and at room temperature. The positions and line widths of the EPR lines were measured as a function of the magnetic field orientation in three orthogonal planes. The data were used to study the electronic properties of the copper ions and to evaluate the exchange interactions between them. Our results are discussed in terms of the electronic pathways for superexchange between copper ions, which are provided by the stacking of pyrazole and phenyl rings of neighboring molecules and by hydrogen−halogen bonds.

Introduction

The magnitude of exchange interactions between metal ions and their relationship to molecular structure and bond properties are areas of considerable interest.[1] Advances in experimental techniques and theoretical models allow the evaluation of small exchange interactions transmitted through long or weak bonds, and systems of high complexity can be studied. This is important to the study of the magnetic interactions observed in biological molecules and their correlation to the structures of these species and the properties of their bonds. In such cases, a measurement of a magnetic interaction within a metalloprotein could provide information to characterize structure and bonds.

Exchange interactions between metal ions transmitted via aromatic rings are important examples and different situations may occur. In some cases, the rings bridge the metal ions and the interaction is transmitted via their σ-electronic skeletons.[2−4] These exchange interactions have relatively large magnitudes ($|J|/k \approx 1-50$ K, where k is the Boltzmann constant).[4] Another case occurs when the metal ions are bound to aromatic rings that are stacked. In these cases, the exchange interactions are transmitted via the overlap of the π-electron orbital of one ring and the π-electron orbital of the neighboring ring[5] and the magnitudes of the exchange interaction are usually much smaller ($|J|/k < 0.1$ K).[6,7]

The role of hydrogen bonds as paths for superexchange interactions has been studied in some copper−amino acid complexes.[8−10] In these cases, the hydrogen bonds involve amino nitrogen and carboxylic oxygen atoms from the amino acids equatorially bound to the copper ions. The magnitudes reported for the exchange parameters are around $|J|/k \sim 0.5$ K. More complex situations where the superexchange bridge involves a hydrogen bond plus other covalent and noncovalent bonds have also been studied.[11]

It has been shown that the electron paramagnetic resonance (EPR) technique offers unique possibilities of performing accurate and selective measurements of exchange interactions having very small magnitudes ($0.0005 \text{ K} \leq |J|/k \leq 0.5$ K).[6,12−18]

* Corresponding author. Fax: (+55-16) 271-3616. E-mail: ciro@if.sc.usp.br.
[†] Universidade de São Paulo.
[‡] UNESP.
[§] Universidad Nacional del Litoral and INTEC.

(1) Kahn, O. *Molecular Magnetism*; VCH Publishers Inc.: New York, 1993.
(2) Kolks, G.; Lippard, S. J.; Waszczak, J. V.; Lilienthal, H. R. *J. Am. Chem. Soc.* **1982**, *104*, 717.
(3) Benelli, C.; Bunting, R. K.; Gatteschi, D.; Zanchini, C. *Inorg. Chem.* **1984**, *23*, 3074.
(4) Bencini, A.; Benelli, C.; Gatteschi, D.; Zanchini, C. *Inorg. Chem.* **1986**, *25*, 398.
(5) Yamauchi, O.; Odani, A.; Masuda, H. *Inorg. Chim. Acta* **1992**, *198−200*, 749.
(6) Goslar, J.; Hilczer, W.; Hoffmann, S. K. *Phys. Status Solidi* **1993**, *175*, 465.
(7) Brondino, C. D.; Calvo, R.; Atria, A. M.; Spodine, E.; Peña, O. *Inorg. Chim. Acta* **1995**, *228*, 261.
(8) Calvo, R.; Passeggi, M. C. G.; Novak, M. A.; Symko, O. G.; Oseroff, S. B.; Nascimento, O. R.; Terrile, M. C. *Phys. Rev. B* **1991**, *43*, 1074.
(9) Siqueira, M. L.; Rapp, R. E.; Calvo, R. *Phys. Rev. B* **1993**, *48*, 3257.
(10) Rapp, R. E.; de Souza, E. P.; Godfrin, H.; Calvo, R. *J. Phys. Condens. Matter* **1995**, *7*, 9595.
(11) Brondino, C. D.; Calvo, R.; Baran, E. *Chem. Phys. Lett.* **1997**, *271*, 51.
(12) Hoffmann, S. K. *Chem. Phys. Lett.* **1983**, *98*, 329.
(13) Hoffmann, S. K.; Goslar, J.; Szczepaniak, L. S. *Phys. Rev. B* **1988**, *37*, 7331.
(14) Levstein, P. R.; Calvo, R. *Inorg. Chem.* **1990**, *29*, 1581.
(15) Brondino, C. D.; Casado, N. M. C.; Passeggi, M. C. G.; Calvo, R. *Inorg. Chem.* **1993**, *32*, 2078.

10.1021/ic990245g CCC: $18.00
Published on Web 09/10/1999

Table 1. Crystal Data and Structure Refinement Details for $CuBr_2(pdmp)_2$ (**1**) and $CuCl_2(pdmp)2$ (**2**)

	1	**2**
empirical formula	$C_{22}Br_2CuH_{24}N_4$	$C_{22}Cl_2CuH_{24}N_4$
a, Å	8.165(5)	8.379(2)
b, Å	10.432(3)	22.630(2)
c, Å	13.385(4)	12.256(2)
β	100.12(4)	98.43(3)
V, Å^3	1122.4(8)	2298.8(7)
Z	2	4
fw	567.81	478.89
space group	$P2_1/n$	$P2_1/c$
T, °C	20(2)	20(2)
λ, Å	0.710 73	0.710 73
ρ_{calcd}, g cm^{-3}	1.680	1.384
μ, cm^{-1}	44.63	11.97
final *R* indices [$I > 2\sigma(I)$]: R1,[a] wR2[b]	0.0620, 0.1535	0.0777, 0.1874
S[a]	1.106	1.098

[a] $R1 = \sum|F_o| - |F_c|/\sum|F_o|$. [b] $wR2 = \{\sum[w(F_o^2 - F_c^2)^2]/\sum[w(F_o^2)^2]\}^{1/2}$. [c] $S = \{\sum[w(F_o^2 - F_c^2)^2]/(n - p)\}^{1/2}$.

These measurements need single-crystal samples and make use of the exchange-narrowing phenomenon.[19−21] To evaluate the exchange interaction parameters from EPR data, detailed single-crystal measurements at more than one microwave frequency are required. The magnitudes of the exchange couplings (*J*) are calculated from the positions and line widths of the spectra obtained from systems having two or more anisotropic metal ions per unit cell.[7,13,15−17] Since exchange narrowing is essentially a temperature-independent phenomenon,[19−21] the great advantage of these experiments is that exchange interactions having very small magnitudes can be measured at room temperature.

We report here the syntheses and the X-ray structures of two new copper complexes with 1-phenyl-3,5-dimethylpyrazole (pdmp) and with bromine (**1**) and chlorine (**2**). Their magnetic properties are studied using EPR spectroscopy in single-crystal samples using two microwave frequencies, 9 and 35 GHz, at room temperature. The different sizes of bromine and chlorine ions introduce changes in the structure of the compounds and in the geometry of the bonds, changing the magnitudes of the exchange interactions. The EPR results are analyzed using the theories of Anderson[19] and Kubo and Tomita[21] for the exchange-narrowing phenomenon. The magnitudes of the exchange interactions between neighbor copper ions are estimated and discussed in terms of the bond properties, in particular the stacking of the aromatic rings and the characteristics of hydrogen−halogen bonds.

Experimental Section

Synthesis and Crystallization of the Compounds. The ligand 1-phenyl-3,5-dimethylpyrazole (pdmp) was obtained as detailed by Mattioli et al.[22] $CuCl_2 \cdot 2H_2O$ and $CuBr_2 \cdot 2H_2O$ of analytical grade were obtained from Merck.

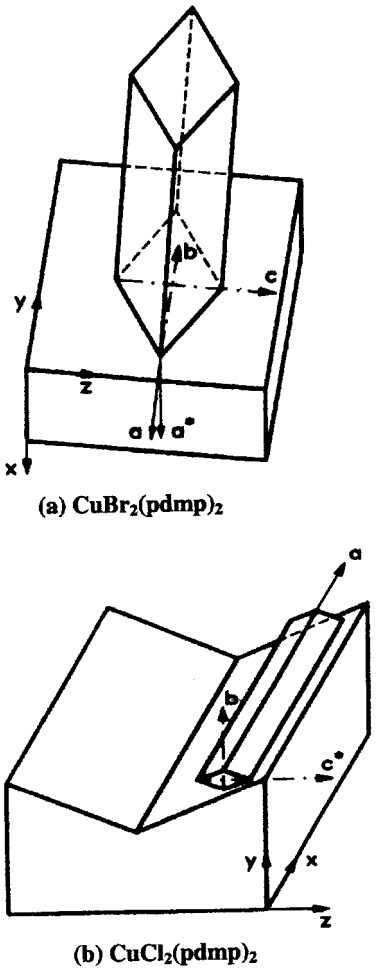

Figure 1. Mounting of the single-crystal samples for the EPR measurements: (a) compound **1**; (b) compound **2**.

$CuCl_2(pdmp)_2$ (2) was obtained[23] by mixing hot ethanolic solutions of $CuCl_2$ and pdmp in the molar proportion M:L = 1:2. The solid was filtered off, washed with cold ethanol, and recrystallized in ethanol. Two compounds appear in the recrystallized material. One is in the form of green microcrystals. The other is studied in this work and consists of well-formed, dark red elongated prismatic crystals. One crystal of maximum and minimum dimensions 0.30 and 0.20 mm was used in the X-ray crystallographic measurements. Larger crystals showing (011) and (100) natural faces were used for the EPR measurements. As explained below, this compound is structurally different from that reported in refs 6 and 23. (The dark green material may be the compound reported in these references. However, this could not be verified using X-rays because of the small size of the crystals obtained.)

$CuBr_2(pdmp)_2$ (1) was obtained using hot ethanolic solutions of $CuBr_2 \cdot 2H_2O$ and pdmp in the molar proportion M:L = 1:2. The crystals are prismatic blocks of two types: dark brown crystals of paramagnetic Cu(II) ions and transparent diamagnetic crystals, which contain Cu(I) ions.[22] Samples of the dark brown crystals having well-defined (011) faces, appropriate for X-ray and EPR measurements, were chosen.

Collection and Analysis of the X-ray Crystallographic Data. Data sets were obtained at room temperature for samples of compounds **1** and **2** with an Enraf-Nonius CAD-4 four-circle diffractometer in the $\theta/2\theta$ mode, using scan widths of $(0.8 + 0.55 \tan \theta)°$ and employing graphite-monochromated Mo Kα radiation ($\lambda = 0.710\ 73$ Å). Unit cell parameters and the orientation matrix for data collection were obtained from 25 automatically centered reflections in the ranges $8 < \theta < 16°$ for compound **1** and $9 < \theta < 18°$ for compound **2**.

Crystal Structure Determination and Refinement. The structures were solved by the standard heavy-atom Patterson method followed by normal difference Fourier techniques. Full-matrix least-squares

(16) Passeggi, M. C. G.; Calvo, R. *J. Magn. Reson., Ser. A* **1995**, *114*, 1.
(17) Martino, D. M.; Passeggi, M. C. G.; Calvo, R. *Phys. Rev. B* **1995**, *52*, 9466.
(18) Martino, D. M.; Passeggi, M. C. G.; Calvo, R.; Nascimento, O. R. *Physica B* **1996**, *225*, 63.
(19) Anderson, P. W. *J. Phys. Soc. Jpn.* **1954**, *9*, 316.
(20) Abragam, A. *The Principles of Nuclear Magnetism*; Clarendon Press: Oxford, U.K., 1959; Chapters IV and X.
(21) Kubo, R.; Tomita, K. *J. Phys. Soc. Jpn.* **1954**, *9*, 888.
(22) Mattioli, M. P. D.; Melios, C. B.; Massabni, A. C.; Molina, M. *Rev. Chim. Miner.* **1984**, *21*, 45.
(23) Francisco, R. H. P.; Lechat, J. R.; Massabni, A. C.; Melios, C. B.; Molina, M. *J. Coord. Chem.* **1980**, *10*, 149.

Table 2. Atomic Coordinates ($\times 10^4$) and Equivalent Isotropic Displacement Parameters ($Å^2 \times 10^3$) for the Atoms Relevant to the Exchange Paths[a]

	x	*y*	*z*	*U*(eq)
	(a) $CuBr_2(pdmp)_2$ (**1**)			
Cu	5000	0	5000	34(1)
Br	2355(1)	1031(1)	4363(1)	49(1)
N(1)	3620(8)	−2615(6)	5067(4)	37(1)
N(2)	4113(8)	−1651(5)	4501(4)	36(1)
C(4)	3380(11)	−3381(8)	3528(5)	46(2)
C(13)	2536(12)	−1520(8)	6425(6)	52(2)
	(b) $CuCl_2(pdmp)_2$ (**2**)			
Cu	2055(1)	3745(1)	7280(1)	45(1)
Cl(1)	562(3)	3854(1)	5601(2)	67(1)
Cl(2)	3569(3)	3633(2)	8934(2)	96(1)
N(11)	−407(8)	2914(3)	7878(5)	50(2)
N(12)	126(8)	3479(3)	7922(5)	46(2)
C(13)	−920(10)	3790(4)	8413(7)	57(2)
C(14)	−2096(10)	3410(5)	8699(7)	58(2)
C(110)	1296(15)	1899(5)	5996(8)	73(3)
C(111)	2384(15)	1602(5)	6719(10)	81(3)
N(21)	4592(8)	4563(3)	6755(5)	52(2)
N(22)	3994(8)	4008(3)	6663(5)	51(2)
C(23)	5033(9)	3690(4)	6175(7)	50(2)
C(24)	6273(10)	4044(5)	5933(7)	61(2)
C(25)	5990(11)	4594(5)	6299(7)	65(3)
C(212)	3639(17)	5659(6)	8799(9)	86(3)

[a] The atoms included are involved in the exchange pathways described in the text. The atomic coordinates for all atoms, including hydrogen atoms, are available as Supporting Information. *U*(eq) is defined as one-third of the trace of the orthogonalized $\mathbf{U}_{ij}$ tensor.

refinement was performed with anisotropic temperature factors for all non-hydrogen atoms; hydrogen atoms were included as fixed contributions at positions calculated on stereochemical grounds, all with an overall isotropic temperature factor that refined to $U = 0.094(11)$ and $0.102(8)$ $Å^2$ for **1** and **2**, respectively. Final R1 and wR2 were 0.0620 and 0.1535 for **1** and 0.0777 and 0.1874 for **2**. A final difference Fourier map showed no features of chemical significance. Programs used were SHELXL93[24] and ORTEP.[25] The scattering factors used were those reported in ref 26. The crystallographic data for compounds **1** and **2** are summarized in Table 1. A full-length table is included with the Supporting Information.

EPR Measurements. Room-temperature EPR spectra of single crystals were obtained at 9 (X-band) and 35 GHz (Q-band), using a Varian E-109 spectrometer equipped with a rotating electromagnet. A (100) natural face of a single-crystal sample of $CuBr_2(pdmp)_2$ of about $2 \times 2 \times 3$ mm^3 was glued with vacuum grease to the ***yz*** face of a cubic sample holder made of cleaved KCl which defines the *xyz* laboratory coordinate system. The ***b*** axis was along the ***y*** direction and $\boldsymbol{a}^* = \boldsymbol{b} \times \boldsymbol{c}$ along the ***x*** direction (Figure 1a). In the case of $CuCl_2(pdmp)_2$, a (011) plane of the sample was glued with vacuum grease to a sample holder having a groove cut at an appropriate angle. The ***a*** axis is oriented along the ***x*** direction of the holder, $\boldsymbol{c}^* = \boldsymbol{a} \times \boldsymbol{b}$ along **z**, and ***b*** along ***y*** (Figure 1b). In this way, the orientation of the magnetic field **B** can be accurately set within the crystal planes $\boldsymbol{a}^*\boldsymbol{b}$, ***cb***, and $\boldsymbol{ca}^*$ for **1** and ***ab***, $\boldsymbol{c}^*\boldsymbol{b}$, and $\boldsymbol{c}^*\boldsymbol{a}$ for **2**, without handling the samples. The crystal axes were located within the planes containing the ***b*** axis, considering the symmetry of the angular variation of the EPR spectra expected in monoclinic crystals. The EPR spectra were acquired and digitized with a microcomputer equipped with a standard data acquisition card. The positions and peak-to-peak line widths of the resonances were calculated by numerical simulation of the spectra assuming Lorentzian line shapes.

(24) Sheldrick, G. M. *SHELXL93: Program for the refinement of crystal structures*; University of Götingen, Germany, 1993.
(25) Johnson, C. K. *ORTEP*; Report ORNL-3794; Oak Ridge National Laboratory: Oak Ridge, TN, 1965.
(26) Hamilton, W. C. *Acta Crystallogr*. **1959**, *12*, 609.

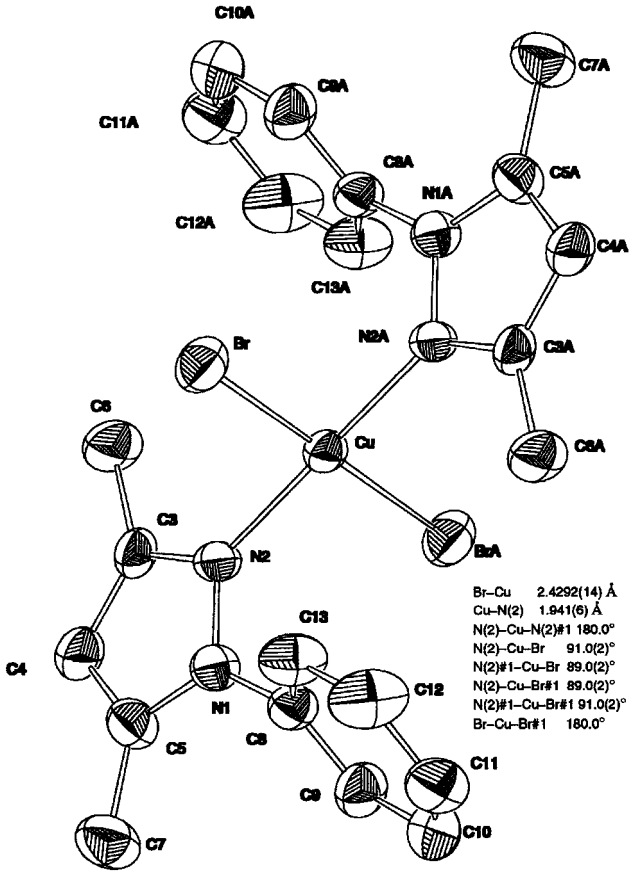

Figure 2. View of the molecular structure of $CuBr_2(pdmp)_2$ (**1**), showing the labeling of the atoms and 50% probability ellipsoids. The inset shows the bond lengths and angles around the Cu(II) ion. The symbol #1 refers to the symmetry transformation which generates the equivalent atoms in compound **1**: $-x + 1, -y, -z + 1$.

Crystallographic Results

Fractional coordinates and equivalent isotropic thermal parameters[26] for the non-hydrogen atoms relevant to the magnetic properties in the compounds **1** and **2** are given in Table 2. Figures 2 and 3 display the molecules of **1** and **2**, respectively, showing the labeling of the atoms and the relevant distances and angles around the copper atoms as insets. Complete listings of refined atomic coordinates and equivalent isotropic thermal parameters, anisotropic thermal parameters for the non-hydrogen atoms, hydrogen atomic coordinates, and bond distances and angles within the pdmp molecule are provided as Supporting Information. Views of the crystal packing of compounds **1** and **2** are shown in Figures 4 and 5.

In compound **1** (Figure 2), the Cu(II) ion is in a site having inversion symmetry with a nearly square planar coordination. As shown by Figure 2, there are two pyrazole nitrogen atoms [d(Cu−N2) = 1.941(6) Å] and two bromine ions [d(Cu−Br) = 2.4292(14) Å] at the corners of the square. The N−Cu−Br angle is 91.0(2)°. The volume of the unit cell is 1122.4(8) $Å^3$, and the volume per asymmetric unit, V/Z, is equal to 561.2 $Å^3$. In compound **2** (Figure 3), the Cu(II) ion is coordinated as in compound **1**, but without having inversion symmetry [d(Cu−N12) = 1.991(6) Å, d(Cu−N22) = 1.981(6) Å; d(Cu−Cl1) = 2.260(2) Å, d(Cu−Cl2) = 2.242(3) Å]. It is important to notice that the two phenyl and pyrazole rings are parallel in compound **1**, as a consequence of the inversion symmetry at the copper positions, but they are not parallel in compound **2**.

Francisco et al.[23] reported a compound with a chemical formula identical to that of **2** but with a different structure. The

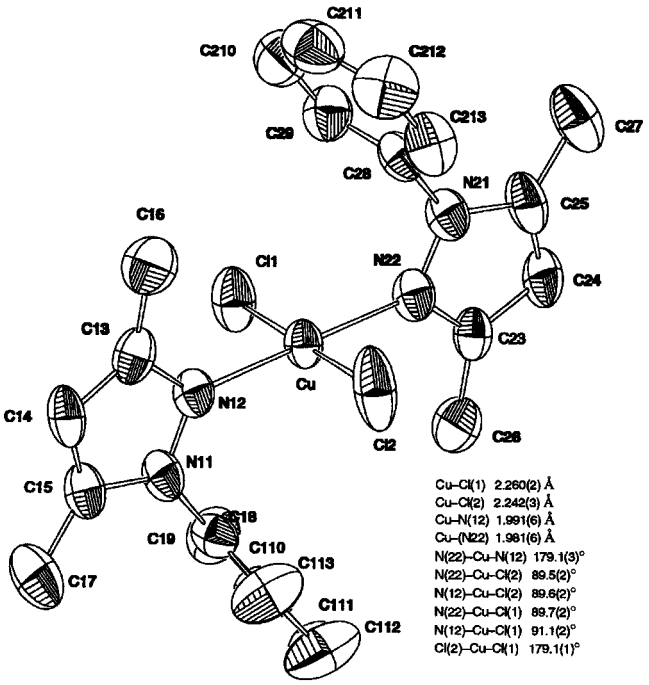

Figure 3. View of the molecular structure of $CuCl_2(pdmp)_2$ (**2**), showing the labeling of the atoms and 50% probability ellipsoids. The inset shows the bond lengths and angles around the Cu(II) ion.

space group is the same, but their compound has $Z = 2$ instead of $Z = 4$, as we obtained. Correspondingly, the volume of the unit cell we report is nearly twice their value. The volume of the unit cell in compound **2** is 2298.8(7) Å^3, and the volume per asymmetric unit, V/Z, is equal to 574.7 Å^3. That reported by Francisco et al. is 1101(1) Å^3 with $V/Z = 550.5$ Å^3. Also, copper ions are sited in inversion centers in their compound but not in ours. The distances between a copper ion and its two chlorine neighbors and that between a copper ion and the two nitrogen neighbors are 2.268 and 1.979 Å, respectively, in the formerly reported compound. In compound **2**, they are 2.260 and 2.242 Å from copper to each chlorine ligand and 1.991 and 1.981 Å from copper to each nitrogen ligand.

EPR Results

The EPR spectra of single-crystal samples of **1** and **2** were obtained at room temperature at 9 and 35 GHz as a function of the orientation of the magnetic field **B**, in the three planes defined in Figure 1a for **1** and in Figure 1b for **2**. In the case of compound **1**, a single anisotropic resonance was observed for any orientation of **B**. In compound **2**, we observed a single anisotropic resonance in the ***c**a*** plane, while two resonances were observed for most orientations of **B** in the ***c**b*** and ***ab*** planes. No hyperfine structure due to the copper nucleus was observed for any orientation of the applied magnetic field in any of the compounds. The line shapes are nearly Lorentzian in all cases, as expected for exchange-narrowed lines.[19−21]

Figure 6a displays the values of g^2 at 9 and 35 GHz for compound **1**. There are small differences in g^2 at the two frequencies. In Figure 7a−f, we plot the g^2 values at each microwave frequency for compound **2**. Parts a and b of Figure 7 display the values of g^2 measured in the ***c**a*** plane. The two resonances observed at both frequencies in the ***ab*** and ***c**b*** planes are shown in Figure 7c−f. The peak-to-peak line width (ΔB_{pp}) data for compound **1** in the three orthogonal planes, at 9 and 35 GHz, are displayed in Figure 6b−d. Figure 6e displays the differences between the line widths observed at 35 and 9 GHz

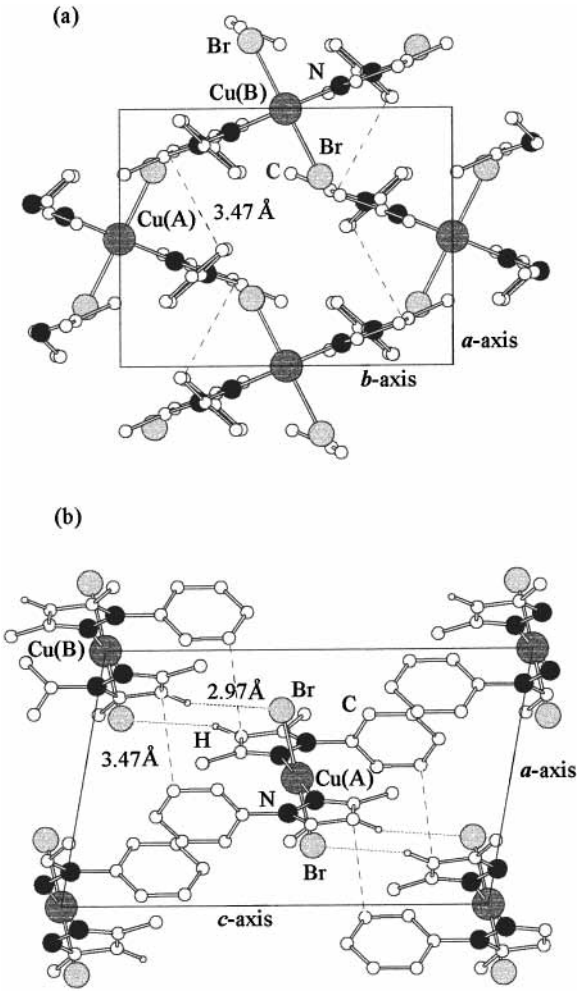

Figure 4. Views of the crystal structure of $CuBr_2(pdmp)_2$ (**1**). Part a is a projection down the ***c*** axis showing the exchange pathway mediated by the partial stacking of the pyrazole (copper B) and phenyl (copper A) rings. The dashed lines indicate the distance between the C_4 atom from the pyrazole ring and the C_{13} atom from the phenyl ring. Part b is a projection down the ***b*** axis showing the same connection discussed in part a (dashed lines) and the hydrogen−halogen bond Br···H−C_4 (dotted lines). These exchange pathways provide the coupling between A and B copper ions (J_{AB}).

in the ***a**b*** and ***cb*** planes. The differences in the ***ca**** plane are smaller. Figure 8a−f shows the line width data in the three planes at each microwave frequency for compound **2**.

Magnetic Properties of the Compounds

The main contributions to the spin Hamiltonian can be written as

$$\mathbf{H} = \mathbf{H}_Z + \mathbf{H}_{ex} = \sum_{i=1}^{N}\sum_{\alpha=1}^{z} \mu_B \mathbf{B}\cdot\boldsymbol{g}_\alpha\cdot\mathbf{S}_{i\alpha} - \sum_{i\alpha,j\beta} J_{i\alpha,j\beta}\mathbf{S}_{i\alpha}\cdot\mathbf{S}_{j\beta} \quad (1)$$

In eq 1, $\boldsymbol{H}_Z$ and $\boldsymbol{H}_{ex}$ are the contributions arising from the Zeeman and exchange interactions. $\mathbf{S}_{i\alpha}$ is the spin operator corresponding to a copper ion in the α position of the ith unit cell ($S = {}^1/_2$). Thus, α = A or B in compound **1** ($Z = 2$) and α = A, B, C, or D in compound **2** ($Z = 4$). As discussed below, we neglect in eq 1 the dipole−dipole interactions, considering the distances between copper ions in the structures of **1** and **2**.

The $\boldsymbol{g}_\alpha$ tensors for different α's are related by the same point group operations as the crystal sites A and B in **1**, and A, B, C, and D in **2**, in the corresponding space groups. Thus, $\boldsymbol{g}_A$ and $\boldsymbol{g}_B$

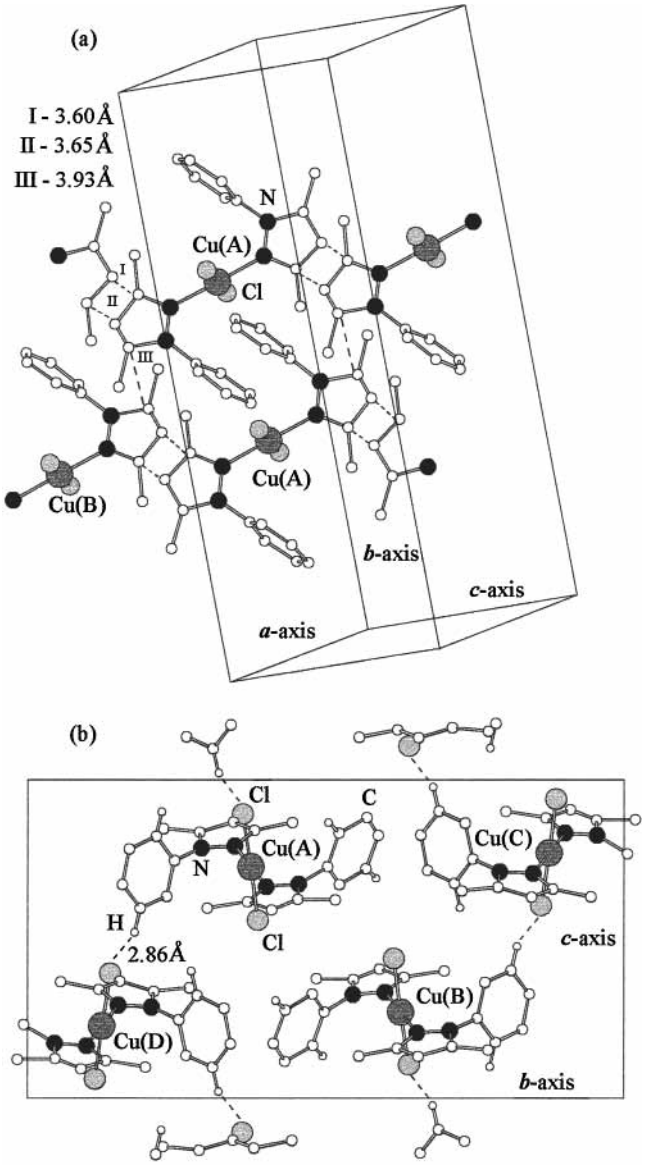

Figure 5. Views of the crystal structure of $CuCl_2(pdmp)_2$ (**2**). Part a is a projection down a convenient axis showing the pyrazole ring stacking (dashed lines) responsible for the couplings either between copper ions A and B (J_{AB}) or between copper ions A and A (J_{AA}). The shortest distances are indicated by I [$d(C_{14}(A)-C_{23}(A)) = 3.60$ Å], II [$d(C_{13}(A)-C_{24}(A)) = 3.65$ Å], and III [$d(C_{25}(A)-C_{25}(B)) = 3.93$ Å]. Part b is a projection down the ***a*** axis showing the hydrogen−halogen bond $Cl\cdots H-C_{110}$ (dashed lines). The Cl−H distance is 2.86 Å, and this exchange pathway provides the coupling between A and D copper ions (J_{AD}), whose magnitude was evaluated in the present work.

are related by a 180° rotation around the ***b*** axis in compound **1**, while $\boldsymbol{g}_A = \boldsymbol{g}_B$ and $\boldsymbol{g}_C = \boldsymbol{g}_D$ (these copper pairs are related by a crystallographic center), with $\boldsymbol{g}_A$, $\boldsymbol{g}_C$ and $\boldsymbol{g}_B$ and $\boldsymbol{g}_D$, related by 180° rotations around ***b*** in compound **2**. Considering only exchange interactions between nearest neighbor copper ions and the symmetry conditions relating the exchange interaction parameters $J_{i\alpha,j\beta}$ in eq 1, only few different parameters contribute. They are discussed below in terms of the crystal structures of the compounds **1** and **2**.

Exchange Network for Compound 1. Inspection of the crystal structure of compound **1** shows that the nearest translated pairs of copper neighbors are at 8.165 Å along the ***a**** axis. However, there is no chemical connection between them that could provide a suitable exchange path. Figure 4a shows that the most relevant electronic paths for superexchange involve

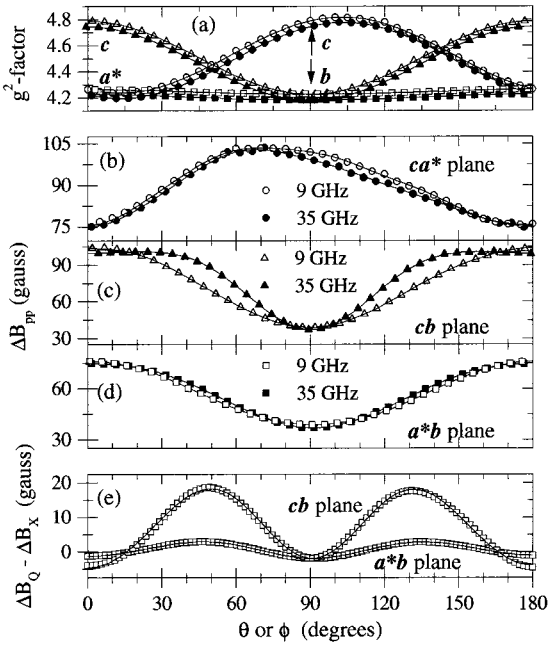

Figure 6. EPR results obtained for $CuBr_2(pdmp)_2$ (**1**): (a) $\mathbf{g}^2$ tensor in the three crystal planes at 9 and 35 GHz (the directions of the crystal axes are shown); (b−d) peak-to-peak line widths (ΔB_{pp}) at both frequencies in the (b) ***ca**** plane (b), the ***cb*** plane (c), and the ***a*b*** plane; (e) differences between the line widths measured at 9 and 35 GHz in the ***a*b*** plane and ***cb*** crystal planes. The solid line in part a was obtained using the function $g^2 = (\boldsymbol{h}\cdot\boldsymbol{g}\cdot\boldsymbol{g}\cdot\boldsymbol{h})$ and the $\boldsymbol{g}^2$ components given in Table 3. Solid lines in parts b−d were obtained using eq 6; the data in part e were are fitted with eq 8.

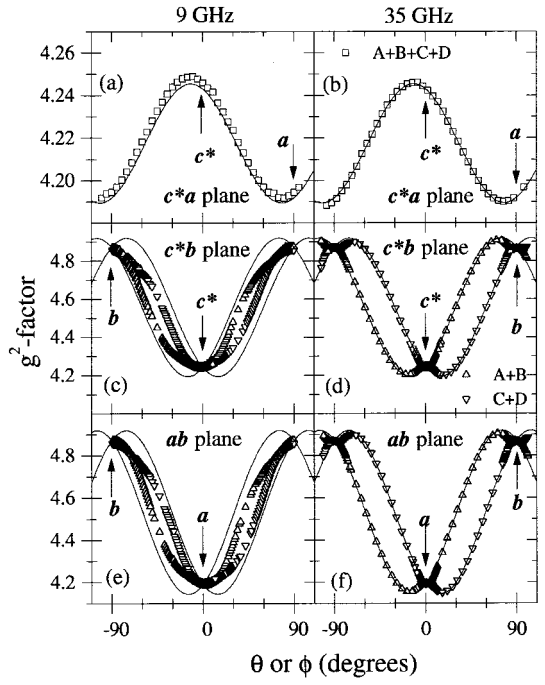

Figure 7. Experimental values of the $\mathbf{g}^2$ tensor for the resonance lines observed for $CuCl_2(pdmp)_2$ in the three crystallographic planes at (a, c, e) 9 GHz and (b, d, f) 35 GHz. The solid lines were obtained with the components of $\boldsymbol{g}^2$ given in Table 3.

pairs of A and B neighbor copper atoms at 8.89 Å in (101) planes. The planes of the pyrazole and phenyl rings bonded to these A and B copper ions are rotated about 23° around the ***c*** axis. The distance between the closest atoms, C_4 from the pyrazole and C_{13} from the phenyl ring, is 3.47 Å (Figure 4a), indicating an overlap of their π electrons. Since other atoms in

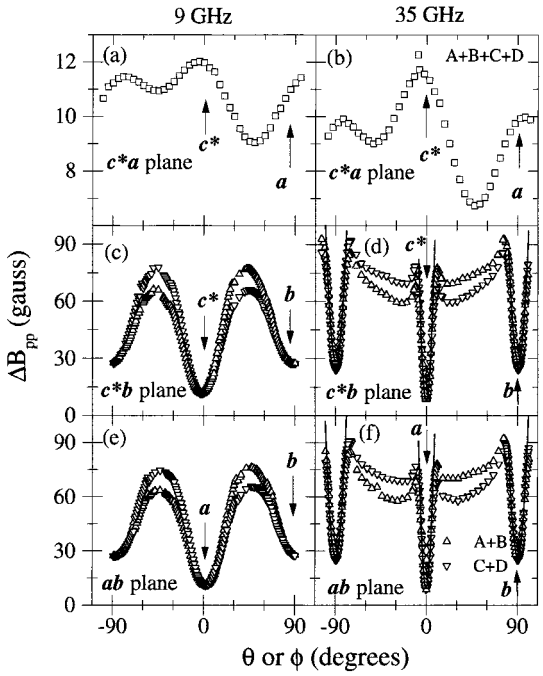

Figure 8. Values of the peak-to-peak line widths (ΔB_{pp}) of the resonance lines observed for $CuCl_2(pdmp)_2$ in the three crystallographic planes at (a, c, e) 9 GHz and (b, d, f) 35 GHz. The solid lines near the positions of the crystal axes in parts d and f were obtained using eq 15.

the rings are farther away, this "ring stacking" is partial. The Br atom and the C_4 of the pyrazole ring provide another possible path for superexchange between copper ions of type A and type B via the hydrogen bond Br···H−C_4 [d(Br−H) = 2.97 Å, d(C_4−H) = 1.01 Å] (Figure 4b). In conclusion, the stacking of pyrazole and phenyl rings and pairs of hydrogen bonds between a pyrazole carbon and bromine ligand to copper provide the superexchange paths in compound **1**. The corresponding exchange parameter will be called J_{AB}. Each copper of type A is coupled to two type B nearest neighbor copper ions at 8.89 Å, and only this contribution to the exchange interaction will be considered in the spin Hamiltonian of eq 1.

Spin Hamiltonian for Compound 1. Considering the space symmetry of compound **1** and taking into account only exchange interactions of a copper ion of type A (B) with its two nearest neighbor copper ions of type B (A), the Zeeman and exchange contributions to the Hamiltonian of eq 1 can be written as

$$\mathbf{H}_Z = \mu_B \mathbf{B}\cdot\sum(\boldsymbol{g}_A\cdot\mathbf{S}_{iA} + \boldsymbol{g}_B\cdot\mathbf{S}_{iB}) = \mu_B\mathbf{B}\cdot(\boldsymbol{g}\cdot\mathbf{S} + \boldsymbol{G}\cdot\mathbf{s}) \quad (2)$$

$$\mathbf{H}_{ex} = -J_{AB}(1)\sum_{i=1}^{N}\sum_{m=1}^{2}\mathbf{S}_{iA}\cdot\mathbf{S}_{mB} \quad (3)$$

where

$$\boldsymbol{g} = {}^1/_2(\boldsymbol{g}_A + \boldsymbol{g}_B) \quad (4)$$

is the average or crystal $\boldsymbol{g}$ tensor; $\mathbf{S} = \sum_i(\mathbf{S}_{iA} + \mathbf{S}_{iB})$ is the total spin of the system (which commutes with $\boldsymbol{H}_{ex}$), $\boldsymbol{G} = {}^1/_2(\boldsymbol{g}_A - \boldsymbol{g}_B)$, and $\mathbf{s} = \sum_i(\mathbf{S}_{iA} - \mathbf{S}_{iB})$ is a spin operator which does not commute with $\boldsymbol{H}_{ex}$. The index i runs over all crystal cells; the index m runs over the two copper neighbors of type B at 8.89 Å and a copper of type A at the ith site. The data for compound **1** in Figure 6 indicate that the exchange interactions are strong enough to collapse the lines corresponding to sites A and B. Thus, in a perturbative approach, the problem can be described as $\boldsymbol{H} = \boldsymbol{H}_0 + \boldsymbol{H}'$, where

$$\mathbf{H}_0 = \mu_B\mathbf{B}\cdot\boldsymbol{g}\cdot\mathbf{S} + \boldsymbol{H}_{ex} \qquad \boldsymbol{H}' = \mu_B\mathbf{B}\cdot\boldsymbol{G}\cdot\mathbf{s} \quad (5)$$

The perturbation $\boldsymbol{H}'$ contains the contribution which, in the absence of exchange interactions, would separate the resonances of sites A and B. When $\boldsymbol{H}_{ex} > \boldsymbol{H}'$, the resonance lines are collapsed and the effect of $\boldsymbol{H}'$ is to broaden these collapsed resonance lines.

Table 3. Components of the Crystal and Molecular $\boldsymbol{g}$ Tensors Obtained from the EPR Data for Compounds **1** and **2**[a]

	$CuBr_2(pdmp)_2$ (**1**)		$CuCl_2(pdmp)_2$ (**2**)
	9 GHz	35 GHz	35 GHz
$(g^2)_{xx}$	4.265(1)	4.2269(1)	4.192(1)
$(g^2)_{yy}$	4.2262(1)	4.181(1)	4.872(2)
$(g^2)_{zz}$	4.789(1)	4.7464(1)	4.243(1)
$(g^2)_{xy}$	0	0	∓0.186(1)
$(g^2)_{zx}$	0.125	0.131	−0.0113(5)
$(g^2)_{zy}$	0	0	∓0.180(2)
$(g^2)_1$	4.237(3)	4.196(2)	4.960(2)
$(g^2)_2$	4.2262(1)	4.181(1)	4.111(1)
$(g^2)_3$	4.817(3)	4.778(2)	4.234(1)
$\mathbf{a}_1$	(0.975(1), 0, −0.221(6))	(0.973(1), 0, −0.231(6))	(0.225, ∓ 0.945, 0.234)
$\mathbf{a}_2$	(0, 1, 0)	(0, 1, 0)	(0.804, ±0.316, 0.503)
$\mathbf{a}_3$	(0.221(6), 0, 0.975(1))	(0.231(6), 0, 0.973(1))	(0.550, ∓ 0.075, −0.832)
g_{N-N}	2.046(1)	2.0351(3)	2.0276(2)
g_{h-h} (h = Cl, Br)	2.0610(9)	2.0513(6)	2.0577(2)
$g_{\|\|}$	2.2013(6)	2.1922(3)	2.2271(4)

[a] $(g^2)_{xx}$, $(g^2)_{yy}$, $(g^2)_{zz}$, $(g^2)_{xy}$, $(g^2)_{zx}$, $(g^2)_{zy}$ are the components of the crystal $\boldsymbol{g}^2$ tensor obtained from fitting the function $g^2 = (\boldsymbol{h}\cdot\boldsymbol{g}\cdot\boldsymbol{g}\cdot\boldsymbol{h})$ to the experimental data. $(g^2)_1$, $(g^2)_2$, $(g^2)_3$ and $\mathbf{a}_1$, $\mathbf{a}_2$, $\mathbf{a}_3$ are the eigenvalues and eigenvectors of the $\boldsymbol{g}^2$ tensor, respectively. For compound **1**, the molecular g values and their principal directions were determined as described in the text. For compound **2**, those values are the ones obtained after diagonalization of the measured $\boldsymbol{g}^2$ tensor. g_{N-N}, g_{h-h}, and $g_{||}$ represent the molecular g values for each compound in the nitrogen−nitrogen, halogen−halogen, and parallel directions, respectively.

Positions of the Resonances. Crystal and Molecular $\boldsymbol{g}$ Tensors for Compound 1. The position of the single resonance observed for **1** is characterized by the average $\boldsymbol{g}$ tensor defined in eq 4. We calculated its components in the laboratory system ($\boldsymbol{xyz} \equiv \boldsymbol{a^*bc}$) by a least-squares fitting of the data in Figure 6a against the function $g^2 = (\boldsymbol{h}\cdot\boldsymbol{g}\cdot\boldsymbol{g}\cdot\boldsymbol{h})$, where $\boldsymbol{h}$ = (sin θ cos ϕ, sin θ sin ϕ, cos θ) is the orientation of the applied magnetic field. These components are given in Table 3, where we include eigenvalues and eigenvectors of the crystal $\boldsymbol{g}$ tensor. The result of the fitting is indicated as solid lines in Figure 6a. As expected, the monoclinic $\boldsymbol{b}$ axis is one principal direction of $\boldsymbol{g}$. The principal axes in the $\boldsymbol{ca^*}$ plane are rotated 12.8 and 13.8° from the $\boldsymbol{x}$ and $\boldsymbol{z}$ axes, at X- and Q-band, respectively (see Figure 6a). The differences between the crystal g values obtained at 9 and 35 GHz (Figure 6a and Table 3) arise from nonsecular contributions to the line positions of the spin Hamiltonian. A simulation of the EPR spectra obtained for powder samples at each microwave frequency gives essentially the same eigenvalues.

To evaluate the components of the molecular $\boldsymbol{g}$ tensors ($\boldsymbol{g}_A$ and $\boldsymbol{g}_B$)[27−29] we assume that one of their eigenvectors is along either the N−Cu−N or the Br−Cu−Br direction or along the

(27) Billing, D. E.; Hathaway, B. J. *J. Chem. Phys.* **1969**, *50*, 1476. Hathaway, B. J.; Billing, D. E. *Coord. Chem. Rev.* **1970**, *5*, 13.
(28) Calvo, R.; Mesa, M. A. *Phys. Rev. B* **1983**, *28*, 1244.
(29) Hoffmann, S. K.; Szczepaniak, L. S. *J. Magn. Reson.* **1983**, *52*, 182.

normal to the N−Cu−Br plane. The rotation matrix for each molecule A and B was calculated under each of these assumptions using eq 4, requiring a wave function of the ground state in the plane of the N and Br ligands attached to copper. The largest eigenvector has to be a direction close to the normal to the N−Cu−Br plane of each molecule, and the g factor within the plane has to be nearly isotropic. This procedure does not assume axial symmetry for the $\boldsymbol{g}$ tensor. The best result gives principal axes of $\boldsymbol{g}_A$ and $\boldsymbol{g}_B$ coincident with the N−Cu−N directions of A and B molecules ($g_{N-N} = 2.0351(3)$, the smallest g value). The other direction is 5° from the Br−Cu−Br direction ($g_{Br-Br} = 2.0513(6)$) and the largest g value is at 5° from the normal to the Br−Cu−N plane ($g_{||} = 2.1922(3)$). This result points to an essentially $d(x^2 - y^2)$ ground orbital state, with a small admixture from the $d(yz)$ orbital. The values of the components of the $\boldsymbol{g}_\alpha$ tensors at 9 and 35 GHz are given in Table 3.

Line Widths of the Resonances and Exchange Interactions for Compound 1. The observed angular variation of the line width for compound **1** occurs within the regime of exchange-collapsed resonances. The contribution of $\boldsymbol{H}'$ of eq 5 to the peak-to-peak line width is in this case[16]

$$\Delta B_{pp}(\theta, \phi) = \sqrt{\frac{2\pi}{3}} \sum_{u=1}^{3} \frac{{\omega_0}^2 \hbar}{g\mu_B \omega_{ex}} \frac{(\boldsymbol{h}\cdot\boldsymbol{g}\cdot\boldsymbol{G}_u\cdot\boldsymbol{h})^2}{g^4(\theta, \phi)} \quad (6)$$

which depends quadratically on the microwave frequency ω_0. The exchange frequency ω_{ex} for $\boldsymbol{H}_{ex}$ of eq 3 is[16]

$$\omega_{ex} = 2^{1/2}|J_{AB}|/\hbar \quad (7)$$

To obtain ω_{ex} using the data in Figure 6 and eq 6, we calculated the difference $\Delta B_{pp}(\theta, \phi)_Q - \Delta B_{pp}(\theta, \phi)_X$ between the line widths measured at Q- and X-bands, in the $\boldsymbol{a}^*\boldsymbol{b}$ and $\boldsymbol{cb}$ crystal planes (Figure 6e). Using eq 6, we obtain

$$\Delta B_{pp}(\theta, \phi)_Q - \Delta B_{pp}(\theta, \phi)_X = \sqrt{\frac{2\pi}{3}} \frac{({\omega_Q}^2 - {\omega_X}^2)\hbar}{g\mu_B \omega_{ex}} \frac{(\boldsymbol{h}\cdot\boldsymbol{g}\cdot\boldsymbol{G}\cdot\boldsymbol{h})^2}{g^4(\theta, \phi)} \quad (8)$$

where

$$(\boldsymbol{h}\cdot\boldsymbol{g}\cdot\boldsymbol{G}\cdot\boldsymbol{h})^2/g^2(\theta, \phi) = [\boldsymbol{g}_A(\theta, \phi) - \boldsymbol{g}_B(\theta, \phi)]^2$$

Equation 8 does not consider frequency-independent contributions to the line width. The exchange frequency ω_{ex} was obtained using eq 8, the data in Figure 6e, and the values of the components of $\boldsymbol{g}_A$ and $\boldsymbol{g}_B$ calculated above. We obtained $\omega_{ex}/2\pi = 5.4(6)$ GHz from the data in the $\boldsymbol{a}^*\boldsymbol{b}$ plane and $\omega_{ex}/2\pi = 4.9(2)$ GHz from the data in the $\boldsymbol{cb}$ plane. Using eq 7 and the average value $\omega_{ex}/2\pi = 5.2(5)$ GHz allows us to obtain

$$|J_{AB}|/k = 0.18(3)\ \text{K}$$

for the exchange interaction between rotated neighbor coppers in compound **1**. The method used does not allow us to obtain the sign of the interaction.

Exchange Network for Compound 2. There are four copper ions in the unit cell of compound **2**, and several superexchange paths are relevant (Figure 5). We chose one type of copper ion (type A) and analyzed the chemical paths connecting this ion to the neighbor copper types A, B, C, and D. All other exchange paths in the structure are related to them by symmetry operations.

There are different types of aromatic ring stacking in this lattice. The pyrazole rings corresponding to copper molecules related by a lattice parameter along the $\boldsymbol{a}$ axis are parallel (A−A stacking). The closest atoms are C_{14} and C_{23} at a distance of 3.60 Å; that between C_{13} and C_{24} is 3.65 Å (Figure 5a). Other ring atoms are farther away, and therefore the stacking A−A is partial. The associated exchange parameter is designated J_{AA}. A pyrazole ring bonded to a copper atom of type A is also parallel and close to the pyrazole ring bonded to a type B neighbor copper (A−B stacking). The carbon atom C_{25} of one ring is 3.93 Å from the carbon atom C_{25} of the other ring, and this distance is the shortest one (Figure 5a). The overlap between their π electrons is smaller than that for the type A−A stacking. The exchange parameter associated to this contact is designated J_{AB}.

The distance between the phenyl carbon atom C_{212} of a type A copper molecule and the phenyl carbon atom C_{111} of the neighbor type C molecule is 3.98 Å, but the planes of these aromatic rings are rotated respect to each other by an angle of 158°. Other distances are larger than 5 Å, indicating that the exchange path connecting types A and C copper atoms is not relevant.

The hydrogen−halogen bond $Cl\cdots H-C_{110}$, involving a hydrogen bond to carbon C_{110} of a phenyl ring and chlorine, having the distances Cl−H = 2.86 Å and C_{110}−H = 0.95 Å, may also contribute as a superexchange path. It connects pairs of copper ions A−D (Figure 5b), and the corresponding exchange parameter is designated J_{AD}. Therefore, each type A copper in compound **2** interacts through two types of stacking with two neighbor copper ions of type B (A and B type coppers are related by an inversion operation; therefore, they give rise to identical EPR spectra). Besides, type A copper interacts through a hydrogen bond with two neighbor copper atoms of type D (A and D type copper atoms are related by a 180° rotation around the $\boldsymbol{b}$ axis, plus an inversion, so they give rise to different but symmetry-related angular variations of the spectra). These couplings between copper atoms will be considered in the spin Hamiltonian of eq 1 for compound **2**. This Hamiltonian will be applied in the two spectral regimes (split and collapsed) observed in the single-crystal EPR spectra of compound **2**.

Spin Hamiltonian for Compound 2. According to the previous discussion, the Zeeman and exchange interactions can be written in this case as

$$\mathbf{H}_Z = \mu_B \sum_i \mathbf{B}\cdot(\boldsymbol{g}_A\cdot\mathbf{S}_{iA} + \boldsymbol{g}_B\cdot\mathbf{S}_{iB} + \boldsymbol{g}_C\cdot\mathbf{S}_{iC} + \boldsymbol{g}_D\cdot\mathbf{S}_{iD}) \quad (9)$$

$$\mathbf{H}_{ex} = J_{AA}\sum_{i,m}\mathbf{S}_{i\alpha}\cdot\mathbf{S}_{m\alpha} + J_{AB}\sum_i[\mathbf{S}_{iA}\cdot\mathbf{S}_{iB} + \mathbf{S}_{iC}\cdot\mathbf{S}_{iD}] + J_{AD}\sum_i[\mathbf{S}_{iA}\cdot\mathbf{S}_{iD} + \mathbf{S}_{iB}\cdot\mathbf{S}_{iC}] \quad (10)$$

where the exchange paths associated with the exchange parameters J_{AA}, J_{AB}, and J_{AD} were described above and $\mathbf{S}_{i\alpha}$ is the spin of the molecule α-positioned in the ith unit cell. The sum over m in the first term is over the nearest neighbor Cu ions to cell i. Since $\boldsymbol{g}_A = \boldsymbol{g}_B$ and $\boldsymbol{g}_C = \boldsymbol{g}_D$ in eq 9, the contributions to $\boldsymbol{H}_{ex}$ proportional to J_{AA} and J_{AB} in eq 10 do not produce any effect on the spectra. The total spin Hamiltonian $\boldsymbol{H} = \boldsymbol{H}_Z + \boldsymbol{H}_{ex}$ may be written again as $\boldsymbol{H} = \boldsymbol{H}_0 + \boldsymbol{H}'$, where $\boldsymbol{H}_0$ and $\boldsymbol{H}'$ depend on which resonance regime (split or collapsed) is being treated.

Split Resonance Regime for Compound 2. In the split resonances regime where two resonance lines are observed

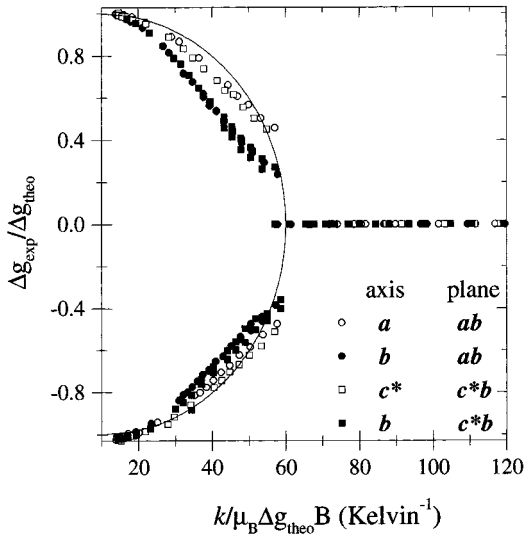

Figure 9. Collapse of the resonance lines in the ***ab*** (circles) and ***c**b*** (squares) planes (35 GHz) of compound **2**. The symbols give the ratio $\Delta g_{exp}/\Delta g_{theo}$ between the difference of the EPR line positions Δg_{exp} measured in each plane and the difference of the line positions Δg_{theo} if there is no exchange interaction. The solid line was obtained using Anderson's model.

(planes ***ab*** and ***c**b***; see Figure 7c−f), the Hamiltonians $\boldsymbol{H}_0$ and $\boldsymbol{H}'$ may be written as

$$\mathbf{H}_0 = \mathbf{H}_Z \tag{11}$$

$$\mathbf{H}' = \mathbf{H}_{ex} \tag{12}$$

Positions of the Resonances for Compound 2. The molecular $\boldsymbol{g}_\alpha$ tensors (α = A, B, C, D) for compound **2** can be obtained directly from the EPR spectra in the split resonance regime at 35 GHz, where the lines are much better resolved. A least-squares fitting of the experimental data in the regions where the resonances are well resolved in the ***ab*** and ***c**b*** planes and for all orientations in the ***c**a*** plane, against the function $g^2 = (\boldsymbol{h}\cdot\boldsymbol{g}\cdot\boldsymbol{g}\cdot\boldsymbol{h})$, leads to the components of the $\boldsymbol{g}_\alpha$ tensors given in Table 3. These results are used to draw the solid lines in Figure 7. The position and collapse of the resonances in the ***ab*** and ***c**b*** planes were also used to evaluate the exchange parameter J_{AD}. In this evaluation, based on Anderson's theory, we used the data of Figure 7c−f in the regions where the resonances are near collapse.[17,18] Figure 9 shows the ratio $\Delta g_{exp}/\Delta g_{theo}$ plotted against the quantity $k/(\mu_B(\Delta g_{theo})\mathbf{B})$. Δg_{exp} is the difference is the g factors observed in the ***ab*** and ***c**b*** planes. Δg_{theo} is that calculated from the molecular $\boldsymbol{g}$ tensors, obtained from the fitting of the angular variation of g^2 (solid lines in Figure 7c−f). k is the Boltzmann constant and **B** the applied magnetic field. Figure 9 shows the collapse of the lines from nonequivalent sites due to the exchange interaction. The two resonances in the ***ab*** plane correspond to the pairs of sites A and D. Thus, from the average value $k/(\mu_B(\Delta g_{theo})\mathbf{B}) = 60 \pm 15$ K^{-1} at the merging points of the two resonances in planes ***ab*** and ***c**b*** (Figure 9), we obtain for compound **2**

$$|J_{AD}|/k = 0.008(3)\ \text{K} \quad (\text{at 9 GHz})$$

$$|J_{AD}|/k = 0.012(3)\ \text{K} \quad (\text{at 35 GHz})$$

Collapsed Resonance Regime for Compound 2. In the collapsed resonances regime (***c**a*** plane and ***ab*** and ***c**b*** planes near the crystal axes), the unperturbed Hamiltonian $\boldsymbol{H}_0$ should be written as

$$\mathbf{H}_0 = \mu_B\mathbf{B}\cdot\boldsymbol{g}\cdot\mathbf{S} + \boldsymbol{H}_{ex} \tag{13}$$

where $\mathbf{S} = \sum\mathbf{S}_{i\alpha}$ is the total spin of the system and $\boldsymbol{g} = (\boldsymbol{g}_A + \boldsymbol{g}_B + \boldsymbol{g}_C + \boldsymbol{g}_D)/4$ is the average $\boldsymbol{g}$ tensor. The exchange interaction $\boldsymbol{H}_{ex}$ commutes with the total spin **S**, and thus $\boldsymbol{H}_0$ gives rise to a single EPR line at the average g factor. The perturbation can be written in this case as

$$\mathbf{H}' = \mu_B\sum_u \mathbf{B}\cdot\boldsymbol{G}_u\cdot\mathbf{s}_u \tag{14}$$

and the introduced broadening of the line is[16]

$$\Delta B_{pp}(\theta,\phi) = \sqrt{\frac{2\pi}{3}}\sum_{u=1}^{3}\frac{\omega_0{}^2\hbar}{g\mu_B\omega_{ex}}\frac{(\boldsymbol{h}\cdot\boldsymbol{g}\cdot\mathbf{G}_u\cdot\boldsymbol{h})^2}{g^4(\theta,\phi)} + \Delta B_{pp}(0) \tag{15}$$

where the $\boldsymbol{G}_u$ are defined in ref 16 and account for the differences among the four molecular g factors. $\Delta B_{pp}(0)$ is a residual line width that considers the small line width observed for the magnetic field along the crystal axes (Figure 8c−f). Due to the space symmetry of compound **2**, and neglecting the interaction between A and C type copper electron spins, the sum over u contains a single term

$$(\boldsymbol{h}\cdot\boldsymbol{g}\cdot\boldsymbol{G}\cdot\boldsymbol{h})^2/g^2(\theta,\phi) = [\boldsymbol{g}_A(\theta,\phi) - \boldsymbol{g}_D(\theta,\phi)]^2$$

Line Widths of the Resonances for Compound 2. A least-squares fitting of the line width data against the function defined in eq 15 for the regions around the crystal axes in the ***ab*** and ***c**b*** planes of compound **2** was performed. The values of the components of the molecular $\boldsymbol{g}$ tensors $\boldsymbol{g}_A$ and $\boldsymbol{g}_D$ evaluated above were used in this calculation. The results of these fittings are shown as solid lines in Figure 8d−f. These values and eq 15 were used to obtain the exchange frequencies and the values of the exchange coupling parameters

$$|J_{AD}|/k = 0.009(2)\ \text{K} \quad (\text{at 9 GHz})$$

$$|J_{AD}|/k = 0.010(2)\ \text{K} \quad (\text{at 35 GHz})$$

Discussion and Conclusions

The *g* Tensor and the Electronic Properties. The ground-state orbital of the copper ions in compounds **1** and **2** is essentially a d($x^2 - y^2$) state. The small differences between the $\boldsymbol{g}^2$ tensors calculated from the data at 9 and 35 GHz are produced by nonsecular contributions that are more important at low frequency. Thus, the values calculated from 35 GHz data are more reliable.

In the case of compound **1**, the resonance lines for the two magnetically different crystal sites are collapsed by the exchange. Thus, the components of the molecular $\boldsymbol{g}$ tensors are chosen from a few possibilities by making assumptions over the orientations of the principal axes. These assumptions are verified in the case of compound **2**, where the resonance lines of the two magnetically different sites are observed, allowing direct measurement of the molecular $\boldsymbol{g}$ tensors. The values obtained for compound **2** from the data at 35 GHz [$g_{||} = 2.2271(5)$, $g_{N-N} = 2.0276(3)$, $g_{Cl-Cl} = 2.0577(2)$] are in good agreement with those obtained in ref 6 for a similar copper environment [$g_{||} = 2.230(5)$, $g_{N-N} = 2.036(2)$, $g_{Cl-Cl} = 2.050(2)$]. The results indicate that the electron ground-state orbital for compounds **1** and **2** is in the plane containing the copper ion and the nitrogen and halogen (Br or Cl) ligands.

Exchange Interactions. From the line width data we obtained $|J_{AB}|/k = 0.18(3)$ K for the exchange interaction between rotated copper ions A and B at 8.89 Å in compound **1**. Two exchange paths connect these ions. The stacking of pyrazole and phenyl rings provides one path (Figure 4a). The hydrogen−halogen bond Br···H−C_4 provides the other path (Figure 4b). They act as a single complex path, and it is not possible to separate their contributions. We will see, however, that a comparison with the results for compound **2** and those of ref 6 allows us to argue in favor of a most relevant contribution.

For compound **2**, we obtain $|J_{AD}|/k = 0.012(3)$ K from the collapse of the resonances in the split resonance regime in the ***ab*** and ***c*b*** planes. We also obtain $|J_{AD}|/k = 0.010(2)$ K from the large increase of the line widths in the neighborhood of the crystal axes in the same planes. Those values are coincident within experimental errors, supporting the methods used in the evaluation. The superexchange path connecting A and D type copper ions at 8.33 Å involves a single hydrogen−halogen bond (Cl···H−C_{110}). The crystal structure of compound **2** indicates that this is the strongest connection between those copper ions. The whole path involves seven diamagnetic atoms between one copper and the other, and the angle Cl···H−C_{110} is 130° (Figure 5b). Thus, the value of $|J_{AD}|$ expected for this weak superexchange pathway should be small, as observed. In ref 6, the coupling between copper ions in a compound having the same molecular formula as **2** but a different structure[23] is discussed. The analyzed exchange path contains the same kind of hydrogen−halogen bond as **2**, but it involves the pyrazole ring instead of the phenyl ring. A weak exchange coupling with a magnitude around 0.006 K was evaluated from the data and attributed to this Cu−Cl−pyrazole−Cu path. This coupling has the same magnitude as the one evaluated by us for compound **2**. Thus, the fact that the compound studied by Goslar et al.[6] (see ref 23 and our crystallographic results) has a larger packing (smaller volume per asymmetric unit) than compound **2** does not seem to play an important role in the magnitude of the exchange interaction. This coupling would be established mainly by the characteristics of the hydrogen bond.

The exchange paths connecting pairs A−B and A−A of copper atoms in compound **2** are essentially stacks of aromatic rings (Figure 5a), but the magnitude of these couplings cannot be evaluated using EPR because the copper atoms involved are magnetically equivalent in all measured crystal planes.

The result for the interaction J_{AD} in compound **2** suggests that the stacking of the aromatic rings is not the leading contribution to the coupling in the case of compound **1**. This stacking is only partial and does not involve the metal directly. On the other hand, there is a pair of hydrogen−halogen bonds connecting an A type copper ion to the neighbor B type copper ion (Figure 4b). This superexchange path involves five diamagnetic atoms between the copper atoms, less than the seven atoms for compound **2**. Also, the angle of the hydrogen−halogen bond Br···H−C_4 is 140°, while it is 130° in compound **2**. The angle H−X−Cu (X = Br, Cl) is 100.8° in compound **2** and 94.3° in compound **1**, which could make the superposition of the p-electron orbital of the halogen ion with the d($x^2 - y^2$) orbital of the copper ion and the σ orbital of the hydrogen more favorable for compound **1**. Furthermore, in compound **1**, both Br atoms of each molecule are involved in the coupling with the other two neighbor molecules (Figure 4b). This does not occur for compound **2**, where only one Cl atom per molecule participates in the coupling (Figure 5b). Hence, the A−B path in compound **1** involves less atoms and the binding angles are more favorable than those for the A−D path in compound **2**. These facts could explain the differences in the magnitudes of the superexchange couplings observed in compounds **1** and **2**.

It is useful to compare the present results for the hydrogen−halogen bonds of compounds **1** and **2** with the results already reported for other copper−amino acid complexes. The halogen−hydrogen bonds can mediate either a coupling strong enough to collapse the EPR lines for any orientation of the applied magnetic field (compound **1**) or a weaker one that would allow us to observe separate resonances of sites A and D (compound **2**). Despite the usual weak character of hydrogen−halogen bonds such as (X···H−C) (X = Br, Cl),[30] the superexchange couplings provided by them could have different magnitudes, as described in this work for compounds **1** and **2**. In the case of compound **1**, the coupling is as effective as those observed for stronger hydrogen bonds of the type O···H−N in copper−amino acid compounds.[17,31] As an example, in copper(II) bis(L-isoleucine),[17] the copper ions are arranged in two symmetry-related layers. The hydrogen bonds O···H−N provide the intralayer superexchange pathways connecting each copper ion to two nonequivalent neighbors, resulting in $|J|/k = 0.14$ K.[17] Another example is the superexchange pathway in a copper(II) bis(α-amino isobutyrate) that was studied in ref 31. In this compound, the copper ions are also distributed in layers and O···H−N hydrogen bonds provide the connection between one copper ion and its four nearest neighbors in the same layer with $|J|/k = 0.22$ K. Hydrogen bonds of the type O···H−N can also provide weak superexchange couplings as obtained in ref 18 for copper(II) bis(glycinate). This interlayer coupling was evaluated $|J|/k = 0.019$ K, suggesting that the hydrogen bond contribution is smaller than this value. In these three Cu(II) compounds, the O···H−N hydrogen bonds are mediated by O and N equatorial ligands on copper (the amine nitrogen from one copper and the carboxyl oxygen from the other copper).

Acknowledgment. This work was supported by the Brazilian agencies Fundação de Amparo à Pesquisa do Estado de São Paulo (FAPESP), Conselho Nacionald de Desenvolvimento Científico e Tecnológico (CNPq), and Fundação Coordenação de Aperfeiçoamento de Pessoal de Nível Superior (CAPES). We also received support of a multinational grant from the Antorchas Foundation.

Supporting Information Available: Listings of structure refinement details, refined atomic coordinates, equivalent isotropic thermal parameters and anisotropic thermal parameters for the non-hydrogen atoms, hydrogen atomic coordinates, and bond distances and angles within the pdmp molecule for both compounds. This material is available free of charge via the Internet at http://pubs.acs.org.

IC990245G

(30) Jeffrey, G. A. *An Introduction to Hydrogen Bonding*; Oxford University Press: Oxford, U.K., 1997.
(31) Calvo, R.; Mesa, M. A.; Oliva, G.; Zukerman-Schpector J.; Nascimento, O. R.; Tovar, M.; Arce, R. *J. Chem. Phys.* **1984**, *81*, 4584.